





RESEARCH ARTICLE | JULY 17 2023

Coupling spin defects in hexagonal boron nitride to a microwave cavity

Thinh N. Tran ; Angus Gale; Benjamin Whitefield; Vladimir Dyakonov; Milos Toth; Igor Aharonovich ; Mehran Kianinia  



Appl. Phys. Lett. 123, 031102 (2023)

<https://doi.org/10.1063/5.0156551>

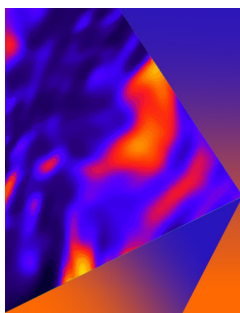


View
Online



Export
Citation

CrossMark



Applied Physics Letters

Special Topic: Mid and Long Wavelength Infrared Photonics, Materials, and Devices

Submit Today



Coupling spin defects in hexagonal boron nitride to a microwave cavity

Cite as: Appl. Phys. Lett. **123**, 031102 (2023); doi: [10.1063/5.0156551](https://doi.org/10.1063/5.0156551)

Submitted: 1 May 2023 · Accepted: 30 June 2023 ·

Published Online: 17 July 2023



View Online



Export Citation



CrossMark

Thinh N. Tran,¹  Angus Gale,¹ Benjamin Whitefield,^{1,2} Vladimir Dyakonov,³ Milos Toth,^{1,2} Igor Aharonovich,^{1,2}  and Mehran Kianinia^{1,a)} 

AFFILIATIONS

¹School of Mathematical and Physical Sciences, Faculty of Science, University of Technology Sydney, Ultimo, New South Wales 2007, Australia

²ARC Centre of Excellence for Transformative Meta-Optical Systems (TMOS), University of Technology Sydney, Ultimo, New South Wales 2007, Australia

³Experimental Physics 6 and Würzburg-Dresden Cluster of Excellence, Julius Maximilian University of Würzburg, Würzburg, Germany

^{a)} Author to whom correspondence should be addressed: mehran.kianinia@uts.edu.au

ABSTRACT

Optically addressable spin defects in hexagonal boron nitride (hBN) have become a promising platform for quantum sensing. While sensitivity of these defects is limited by their interactions with the spin environment in hBN, inefficient microwave delivery can further reduce their sensitivity. Here, we design and fabricate a microwave double arc resonator for efficient transferring of the microwave field at 3.8 GHz. The spin transitions in the ground state of V_B^- are coupled to the frequency of the microwave cavity, which result in enhanced optically detected magnetic resonance (ODMR) contrast. In addition, the linewidth of the ODMR signal further reduces, achieving a magnetic field sensitivity as low as $42.4 \mu\text{T}/\sqrt{\text{Hz}}$. Our robust and scalable device engineering is promising for future employment of spin defects in hBN for quantum sensing.

© 2023 Author(s). All article content, except where otherwise noted, is licensed under a Creative Commons Attribution (CC BY) license (<http://creativecommons.org/licenses/by/4.0/>). <https://doi.org/10.1063/5.0156551>

Optically active spin defects constitute the quantum hardware for applications in sensing and communication technologies.^{1–5} Among existing solid state materials, hexagonal boron nitride, a wideband gap two dimensional material, has been shown to host variety of spin defects at room temperature.^{6–8} Recently, a class of spin defects—namely, the negatively charged boron vacancy V_B^- —in hexagonal boron nitride (hBN) has emerged as a promising candidate for quantum sensing applications.^{6,9} The V_B^- emits at ~ 810 nm under excitation with a 532 nm laser and has ground state spin transitions between $|0\rangle$ and $|\pm 1\rangle$ at ~ 3.48 and 3.58 GHz.⁶ Quantum sensing of strain, magnetic, and electric fields have been demonstrated using spin properties of the defects, and the coherent control of the spin state in pulse measurement has been used to sense paramagnetic particles in a microfluidic channel.^{9–15} Furthermore, more excitement has been brought to the field by the possibility of achieving very thin or monolayer hBN as a host for spin defects, which reduces the quantum sensor to sample distance to minimum possible, opening more avenues for performing quantum sensing.¹⁶ With these fundamental attributes, V_B^- defects have the potential to become an important tool to study

physical properties of emerging 2D materials, devices, and heterostructures.^{9,10,17}

In order to control and manipulate spin state using microwave (MW) field, metal waveguides, such as gold stripes, are commonly used.^{12,13,18} Microwave delivery can be achieved in these structures by directly transferring a hBN flake on top of the metal strip. However, it is an inefficient and lossy method for coupling the MW field to the spin defects. In an alternative approach, one can design and engineer a microwave cavity that resonates with the transitions of the defect spin states.^{19–24} Such a cavity is posed to enhance optically detected magnetic resonance (ODMR) contrast and prevent microwave power broadening, thus enhancing the spin sensitivity. In turn, the improvement of ODMR contrast and sensitivity of V_B^- defects in hBN can boost their application for sensing applications.

In this work, we effectively facilitate the process of designing and fabricating a microwave resonator close to the transition of V_B^- , from $|0\rangle$ to $|+1\rangle$ spin sublevels in the ground state. The microwave resonators were engineered by low cost printed circuit boards (PCBs), which can easily be tuned by changing the inner arc radius. Our results show

the improvement in ODMR contrast and the magnetic field detection sensitivity of the hybrid structure, paving the way to integrating a microwave cavity to spin defects in hBN for ultra-high sensitive quantum sensing.

To create the V_B^- defects, we have used a low energy nitrogen ion beam at 30 KeV to generate as shown in Fig. 1(a). First, hBN flakes were exfoliated from bulk crystal on a clean silicon substrate with a thin layer of thermal oxide and further cleaned in a UV ozone chamber for 15 min to remove any organic residuals from the surface. During the implantation, the nitrogen ion beam was maintained at 2×10^{16} ion-cm $^{-2}$ with ion current at 21.9 pA.^{25–28}

The V_B^- defects are a spin 1 system with a triplet ground state separated as shown schematically in Fig. 1(b). The degeneracy of the $|\pm 1\rangle$ states is lifted at zero external magnetic field. This is evident with the two distinct resonances, $\nu_{1,2}$ in the ODMR spectra of the V_B^- defect. The resonance frequencies, $\nu_{1,2}$, are generalized under external magnetic field (B) as $\nu_{1,2} = D_{gs}/h + (1/h)\sqrt{E_{gs}^2 + (g\mu_B B)^2}$, where D_{gs} and E_{gs} are zero-field splitting parameters, g is the Landé factor, μ_B is the Bohr magneton, and h is the Planck's constant. Without an external magnetic field, the two resonance frequencies only split about $E_{gs}/h \approx 50$ MHz, which could adversely affect the characterization of the microwave resonator and the V_B^- defects. Therefore, we intentionally designed the resonance frequency of the resonator, ω_c at ≈ 3.8 GHz and tune the transition between $|0\rangle$ and $|+1\rangle$, ν_2 , to match f_c with an external magnetic field [Fig. 1(b)].

To confirm the successful generation of the V_B^- defects, a confocal microscopy characterization was carried out. The optical setup used in this study consists of a continuous wave 532 nm laser focused on the sample using a 0.9 NA objective. The photoluminescence is collected through the same objective into a multimode fiber directed into either single photon detectors or spectrometer. Under excitation with 2 mW of laser, the emission from V_B^- defects centered at ~ 810 nm was detected as shown in Fig. 1(c).^{6,27}

Next, the hBN flake was transferred on to the fabricated microwave cavity with a resonance frequency at 3.8 GHz. The device was mounted on the optical setup and connected to an RF generator and amplifier to sweep the microwave frequency between 3.4 and 4 GHz.

A small magnet was used in order to tune the transition between $|0\rangle$ and $|+1\rangle$ of the V_B^- ground state to the cavity resonance frequency through the Zeeman effect.

Figure 2(a) shows the double arc resonator on a PCB (Rogers 4350B substrate) with a compact size ($\sim 28 \times 15$ mm 2). The resonator consists of two closely separated arcs by a small gap. The microwave signal is delivered through a standard 50 Ω microstrip line, which forms a capacitor with the double gap-arc by a small distance. The design was inspired by the proposal from Bayat *et al.*¹⁹ used for uniform coupling of microwave field to NV centers within a millimeter size diamond crystal. To further characterize the design and fine-tune resonance frequency, the electromagnetic numerical simulations (CST Studio Suite) were used. Figure 2(b) shows the simulated magnetic field strength distribution at the frequency of 3.78 GHz without any loads. In this configuration, the magnetic field concentrates along the rims of the outer arc.

The resonance frequency of the resonator was calculated from the simulated results of return loss (S_{11}) of the resonator as shown in Fig. 2(c) (orange curve) and confirmed experimentally by measuring the transmission of the resonator (blue curve). The resonance has a marginally lower Q factor of ~ 65 and a resonance frequency of ~ 3.8 GHz. These differences are due to PCB fabrication imperfection and the capacitive coupling during the measurement. The design parameters of the resonator are given in Table I. The resonance frequency of the resonators can be tuned by modifying the radius of the inner arc r_1 . Seven resonators with different inner radii were fabricated and measured to identify the resonance frequency. The correlation between the resonance frequencies and the inner radii is shown in Fig. 2(d). This result shows a linear dependence between the resonance frequency and the inner radius with a slope of -0.63 GHz/mm.

To couple the V_B^- defects to the resonator, the hBN flake containing the defects was transferred directly onto the PCB, in the region where the microwave field is strongest at the rim of the upper arc. To shift the resonance frequency (ν_2) of V_B^- defects to the cavity mode, a small magnetic field needs to be applied perpendicularly to the flake. Figure 3(a) shows ODMR spectra of V_B^- in the absence of an external magnetic field (blue) and when the signal is brought to the resonance of the microwave cavity under ~ 10 mT of an external magnetic field. ODMR measurement has been performed under continuous

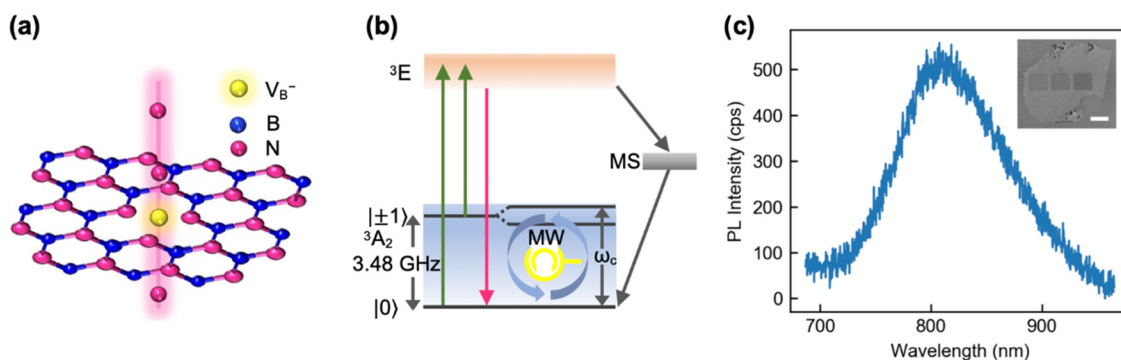


FIG. 1. Spin defects in hBN. (a) Creation of V_B^- by nitrogen (N) ion beam implantation into the hBN lattice. (b) Electronic level structure of V_B^- in hBN with zero-field splitting at ground state $E_{gs} = 3.48$ GHz. By using an external magnetic field, the ground state spin triplet is split into transitions between $m_s = +1$ and $m_s = 0$ to match the resonance frequency of the microwave cavity (ω_c). (c) Photoluminescence spectrum from representative V_B^- defects in hBN. Inset: the scanning electron microscope (SEM) of a hBN flake after N ion beam radiation on areas of $50 \times 50 \mu\text{m}^2$ (scale bar: $50 \mu\text{m}$).

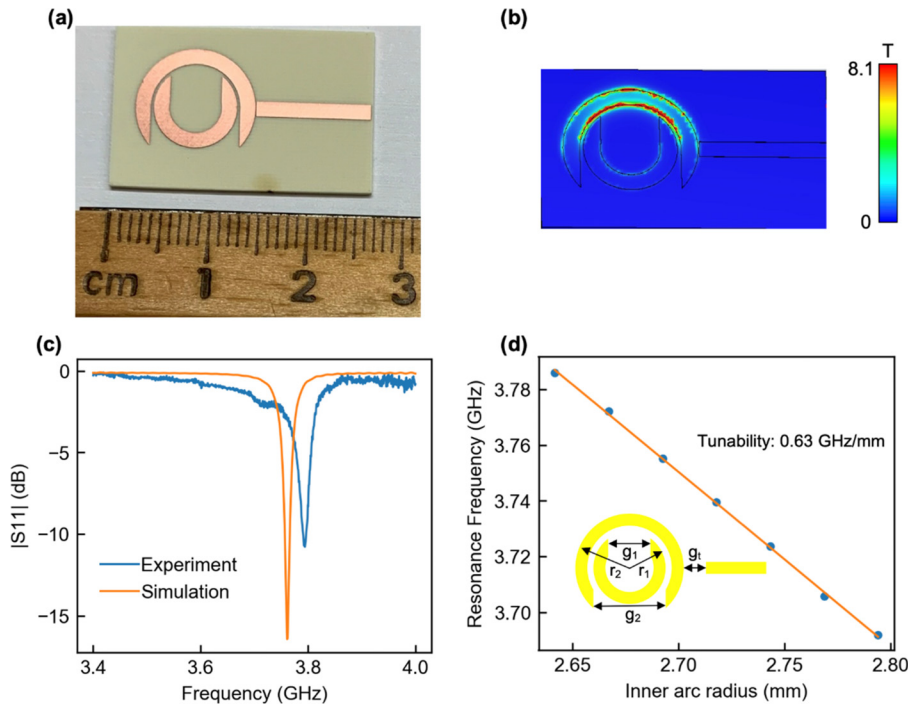


FIG. 2. Microwave resonator characterizations. (a) A double arc resonator on a PCB. (b) Simulated magnetic field strength distribution of the resonator with the intensity color bar on the right. (c) Simulated (orange) and measured (blue) return loss (S_{11}) of a resonator with geometrical parameters listed in the text. (d) Resonance frequency of the double arc resonator as a function of the radius of the inner arc together with the 2D design of the resonator. r_1 and r_2 are the radii of the inner and outer arcs, respectively; g_1 and g_2 are the cut width of the inner and outer arcs, respectively; g_t is the distance between the transmission line to the outer arc.

microwave and laser excitation. The ODMR contrast is increasing to $\sim 7\%$ employing the cavity resonance, compared to a pristine contrast of $\sim 1.7\%$, under the same microwave power (15 dBm). Improvement in ODMR contrast and magnetic field sensitivity was also reported by coupling NV centers in diamond to microwave cavities.^{19–21,29–31}

To further corroborate the coupling strength of V_B^- defects into the microwave resonator, we perform ODMR measurements under different microwave powers. Figures 3(b) and 3(c) show the ODMR contrast and linewidth as a function of microwave power. All experiments were carried out under laser excitation with power of 2 mW. The ODMR contrast increases significantly when the B field is applied to tune the ODMR resonance to the cavity mode. Notably, even under very low microwave powers (~ -20 dBm), where the signal is nondetectable under zero magnetic field, the detection becomes feasible if the ODMR signal is brought to the cavity mode by application of an external magnetic field. While this limits the application of the device for detecting static magnetic field by monitoring the Zeeman effect, the improved contrast can be useful for detection of an AC magnetic field through relaxometry method.³² At the maximum microwave power of 15 dBm, the ODMR contrast increases about 3.5 times

($\sim 6.8\%$), accompanied by $\sim 20\%$ linewidth reduction reaching contrast of 6.8% and linewidth of 104 MHz in our sample. Note that the ODMR linewidth or contrast does not change with the applied magnetic field (>10 mT) and the improvement in the contrast or reduction in linewidth are due to the microwave cavity effect.

With the enhancement of ODMR contrast and reduction in linewidth broadening under high microwave power, the magnetic field sensitivity is expected to be improved. The magnetic field sensitivity is defined by the ODMR contrast C , average photon count rate R and the linewidth $\Delta\nu$ as the following equation:³³

$$\eta_B \approx P_F \frac{h}{g\mu_B} \frac{\Delta\nu}{C\sqrt{R}},$$

where P_F is a numerical parameter related to line shape profile. In our case, $P_F \approx 0.7$ for a Gaussian profile. Given the measured photon count rates, ODMR contrasts, and linewidths, the magnetic sensitivities can be calculated as shown in Fig. 3(d). We observed an enhancement of about ~ 5 times in magnetic sensitivity, which reaches $\sim 42.4 \mu\text{T}/\sqrt{\text{Hz}}$ with the microwave resonator. This is slightly lower compared to the reported 13 times improvement in sensitivity of NV

TABLE I. Design parameters for the resonator with Q factor of ~ 90 and resonant frequency of 3.78 GHz.

Parameters			Comments
$\epsilon_r \sim 3.48$	$r_1 \sim 2.79$ mm	$g_t \sim 101$ μm	$\epsilon_r, t_{Cu}, \tan(\sigma), w, g_t, r_1, r_2, g_1,$ and g_2 are dielectric constant of the PCB, thickness of the copper layer on the PCB, loss tangent of the PCB material, width of copper traces, inner radius, outer radius, coupling gap, gap between the rings, and cut width of the inner and outer arcs, respectively
$t_{Cu} \sim 89$ μm	$r_2 \sim 4.55$ mm	$g_2 \sim 9.1$ mm	
$\tan(\sigma) \sim 0.0037$	$g_1 \sim 5.13$ mm	$w \sim 1.6$ mm	

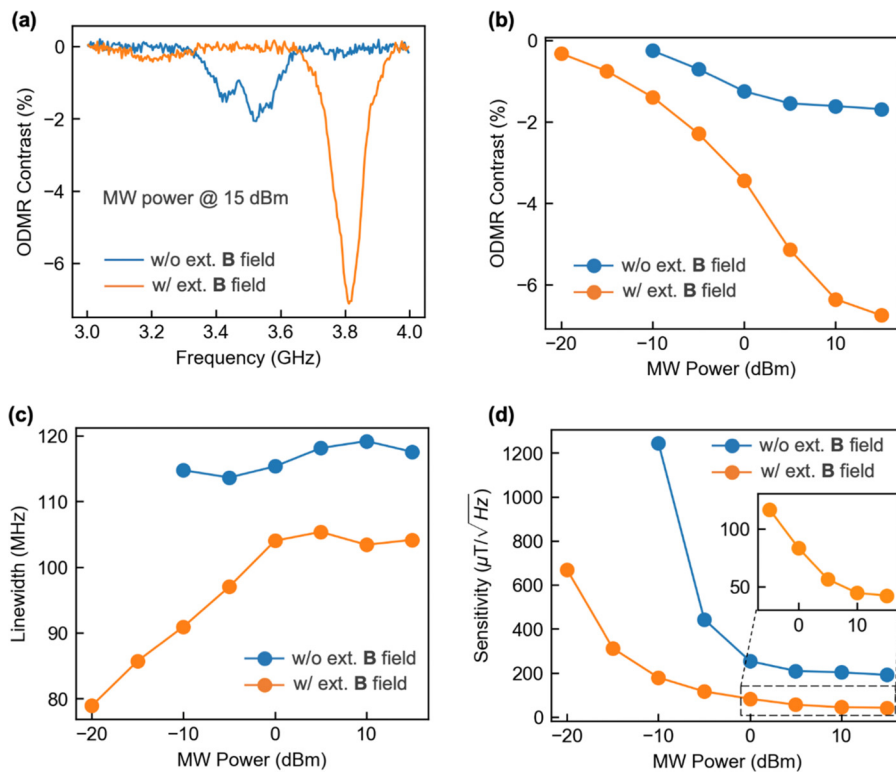


FIG. 3. ODMR comparison between with (orange) and without (blue) an external magnetic field where the V_B^- transition matched to the cavity mode. (a) ODMR spectrum under $B=0$ and $B=10$ mT magnetic fields at the same microwave power (15 dBm). (b) ODMR contrasts, (c) linewidths, and (d) magnetic field sensitivity at different microwave powers at $B=0$ or $B=10$ mT. The inset in (d) shows a zoom-in of the sensitivity from 0 to 15 dBm when an external magnetic field is applied.

center²⁹ by coupling to a microwave cavity. Lower coupling into the cavity mode is expected from V_B^- defects in hBN since spin resonances are much broader due to the hyperfine coupling to neighboring nitrogen atoms, resulting in less improvement compared to NV centers in diamond.

To summarize, we have demonstrated the coupling of spin defects (V_B^-) in hBN to a microwave resonator. The higher ODMR contrast ($\sim 6.8\%$) and narrower linewidth (~ 104 MHz) were achieved due to the coupling between the microwave resonator and the transition frequency of the V_B^- between $|0\rangle$ and $|+1\rangle$ states under external magnetic field. Furthermore, the detectable magnetic field sensitivity can be reduced to as low as $42.2 \mu\text{T}/\sqrt{\text{Hz}}$, making it appropriate for detection of small magnetic fields. The high sensitivity of the coupled system is important for quantum sensing application using spin defects in a layered hBN material.

This work was supported by the Australian Research Council (Nos. CE200100010 and FT220100053) and the Office of Naval Research Global (No. N62909-22-1-2028).

AUTHOR DECLARATIONS

Conflict of Interest

The authors have no conflicts to disclose.

Author Contributions

Thin N. Tran: Data curation (equal); Project administration (equal); Writing – original draft (equal). **Angus Gale:** Data curation (equal);

Investigation (equal); Resources (equal); Writing – original draft (equal). **Benjamin Whitefield:** Data curation (equal); Methodology (equal); Writing – original draft (equal). **Vladimir Dyakonov:** Validation (equal); Writing – review & editing (equal). **Milos Toth:** Supervision (equal); Writing – review & editing (equal). **Igor Aharonovich:** Supervision (equal); Writing – original draft (equal); Writing – review & editing (equal). **Mehran Kianinia:** Conceptualization (equal); Supervision (equal); Writing – original draft (equal); Writing – review & editing (equal).

DATA AVAILABILITY

The data that support the findings of this study are available from the corresponding author upon reasonable request.

REFERENCES

- ¹G. Wolfowicz, F. J. Heremans, C. P. Anderson *et al.*, *Nat. Rev. Mater.* **6**(10), 906 (2021).
- ²M. Atatüre, D. Englund, N. Vamivakas *et al.*, *Nat. Rev. Mater.* **3**(5), 38 (2018).
- ³D. D. Awschalom, R. Hanson, J. Wrachtrup *et al.*, *Nat. Photonics* **12**(9), 516 (2018).
- ⁴F. Casola, T. van der Sar, and A. Yacoby, *Nat. Rev. Mater.* **3**(1), 17088 (2018).
- ⁵D. Le Sage, K. Arai, D. R. Glenn *et al.*, *Nature* **496**(7446), 486 (2013).
- ⁶A. Gottscholl, M. Kianinia, V. Soltamov *et al.*, *Nat. Mater.* **19**(5), 540 (2020).
- ⁷N. Mendelson, D. Chugh, J. R. Reimers *et al.*, *Nat. Mater.* **20**(3), 321 (2021).
- ⁸H. L. Stern, Q. Gu, J. Jarman *et al.*, *Nat. Commun.* **13**(1), 618 (2022).
- ⁹A. J. Healey, S. C. Scholten, T. Yang *et al.*, *Nat. Phys.* **19**, 87–91 (2023).
- ¹⁰M. Huang, J. Zhou, D. Chen *et al.*, *Nat. Commun.* **13**(1), 5369 (2022).
- ¹¹W. Liu, V. Ivády, Z.-P. Li *et al.*, *Nat. Commun.* **13**(1), 5713 (2022).
- ¹²X. Gao, S. Vaidya, K. Li *et al.*, *Nat. Mater.* **21**(9), 1024 (2022).

- ¹³X. Gao, B. Jiang, A. E. Llacsahuanga Allica *et al.*, *Nano Lett.* **21**(18), 7708 (2021).
- ¹⁴A. Gottscholl, M. Diez, V. Soltamov *et al.*, *Nat. Commun.* **12**(1), 4480 (2021).
- ¹⁵W. Liu, Z.-P. Li, Y. Z. Yang *et al.*, *ACS Photonics* **8**(7), 1889 (2021).
- ¹⁶A. Durand, T. Clua-Provost, F. Fabre *et al.*, [arXiv:2304.12071](https://arxiv.org/abs/2304.12071) (2023).
- ¹⁷P. Kumar, F. Fabre, A. Durand *et al.*, *Phys. Rev. Appl.* **18**(6), L061002 (2022).
- ¹⁸P. Yu, H. Sun, M. Wang *et al.*, *Nano Lett.* **22**(9), 3545 (2022).
- ¹⁹K. Bayat, J. Choy, M. Farrokh Baroughi *et al.*, *Nano Lett.* **14**(3), 1208 (2014).
- ²⁰K. Sasaki, Y. Monnai, S. Saijo *et al.*, *Rev. Sci. Instrum.* **87**(5), 053904 (2016).
- ²¹Y. Chen, H. Guo, W. Li *et al.*, *Appl. Phys. Express* **11**(12), 123001 (2018).
- ²²M. Mrózek, J. Mlynarczyk, D. S. Rudnicki *et al.*, *Appl. Phys. Lett.* **107**(1), 013505 (2015).
- ²³Y. Masuyama, K. Mizuno, H. Ozawa *et al.*, *Rev. Sci. Instrum.* **89**(12), 125007 (2018).
- ²⁴E. R. Eisenach, J. F. Barry, L. M. Pham *et al.*, *Rev. Sci. Instrum.* **89**(9), 094705 (2018).
- ²⁵M. Kianinia, S. White, J. E. Fröch *et al.*, *ACS Photonics* **7**(8), 2147 (2020).
- ²⁶N.-J. Guo, W. Liu, Z.-P. Li *et al.*, *ACS Omega* **7**(2), 1733 (2022).
- ²⁷H. Liang, Y. Chen, C. Yang *et al.*, *Adv. Opt. Mater.* **11**(1), 2201941 (2023).
- ²⁸T. Suzuki, Y. Yamazaki, T. Taniguchi *et al.*, *Appl. Phys. Express* **16**(3), 032006 (2023).
- ²⁹Y. Wang, Y. Liu, H. Guo *et al.*, *Appl. Phys. Express* **13**(11), 112002 (2020).
- ³⁰X. Yang, N. Zhang, H. Yuan *et al.*, *AIP Adv.* **9**(7), 015106 (2019).
- ³¹E. R. Eisenach, J. F. Barry, M. F. O'Keeffe *et al.*, *Nat. Commun.* **12**(1), 1357 (2021).
- ³²X. Gao, S. Vaidya, P. Ju *et al.*, [arXiv:2303.02326](https://arxiv.org/abs/2303.02326) (2023).
- ³³A. Dréau, M. Lesik, L. Rondin *et al.*, *Phys. Rev. B* **84**(19), 195204 (2011).